Eur Biophys J (1999) 28: 243–253

ARTICLE

Erkut Inan Iseri · Demet Gülen

Electronic excited states and excitation transfer kinetics in the Fenna-Matthews-Olson protein of the photosynthetic bacterium *Prosthecochloris aestuarii* at low temperatures

Received: 12 June 1998 / Revised version: 19 October 1998 / Accepted: 30 November 1998

Abstract The molecular structure-function relationship of the Fenna-Matthews-Olson light-harvesting complex of the photosynthetic green bacterium *Prosthecochloris aestuarii* has been investigated. It has been assumed that the electronic excited states responsible for the function (transfer of electronic excitation energy) result from the dipole-dipole interactions between the bacteriochlorophyll molecules bound to the polypeptide chain of the complex at a specific three-dimensional geometry. The molecular structure-electronic excited states relationship has been addressed on the basis of simultaneous simulations of several spectroscopic observations. Current electronic excited state models for the Fenna-Matthews-Olson complex have generally been based on obtaining an optimal match between the information contents of the optical steady-state spectra and the bacteriochlorophyll organization. Recent kinetic and spectral information gathered from ultrafast time-resolved measurements have not yet been used effectively for further refinement of the excited state models and for quantification of the relation between the excited states and the energy transfer processes. In this study, we have searched for a model that not only can explain the key features of several steady-state spectra but also the temporal and spectral evolution observed in a recent absorption difference experiment and we have discussed the implications of this model for equilibration of the electronic excitation energy in systems at low temperatures.

Key words Photosynthesis · Fenna-Matthews-Olson protein · Excitons · Optical steady-state spectra · Absorption difference spectra

Abbreviations *ABS* Absorption · *ADS* Absorption difference spectrum/spectral · *BChl* Bacteriochlorophyll *a* · *CD* Circular dichroism · *EES* Electronic excited state · *ESA* Excited state absorption · *FMO* Fenna-Matthews-Olson · *LD* Linear dichroism · *LHC* Light-harvesting complex · *PB* Photobleaching · *RC* Reaction center · *SE* Stimulated emission · *STAD* Singlet-triplet absorption difference

E.I. Iseri · D. Gülen (✉)
Department of Physics, Middle East Technical University, TR-06531 Ankara, Turkey
e-mail: dgul@rorqual.cc.metu.edu.tr

Introduction

Two primary steps of photosynthesis are the creation and transfer of excitation energy in the light-harvesting complex (LHC) and the use of this energy for driving electron transfer processes in the reaction center (RC). A series of electron transfer processes in the RC leads to a charge separation that initiates the photochemistry of photosynthesis. The transfer of energy in the LHC and the subsequent charge separation in the RC take place in a picosecond time scale and are very efficient.

The fundamental questions about these primary steps are: what are the structures of the LHC/RC complexes and what are the physical mechanisms of the energy and electron transfer processes?

Owing to recent advances in ultrafast spectroscopy, X-ray crystallography, and molecular genetics, these questions are now yielding answers (for recent reviews see Fleming and van Grondelle 1994; van Grondelle et al. 1994). A considerable amount of information on these questions can be obtained by setting the connection between the structure and spectroscopy through modeling of the steady-state and time-resolved spectral properties.

In this study the structure-spectroscopy relationship for a particular LHC, the bacteriochlorophyll *a* (BChl) protein complex of the green bacterium *Prosthecochloris aestuarii*, commonly referred to as the Fenna-Matthews-Olson (FMO) complex (Fenna and Matthews 1975; Tronrud et al. 1986), will be investigated. Since the first atomic resolution model of the FMO complex became available in 1975, the question of the relationship between the BChl organization, electronic excited states (EES), and energy transfer processes has been addressed by numerous theoretical and experimental studies (for comprehensive reviews, see Pearlstein 1991; Blankenship et al. 1995).

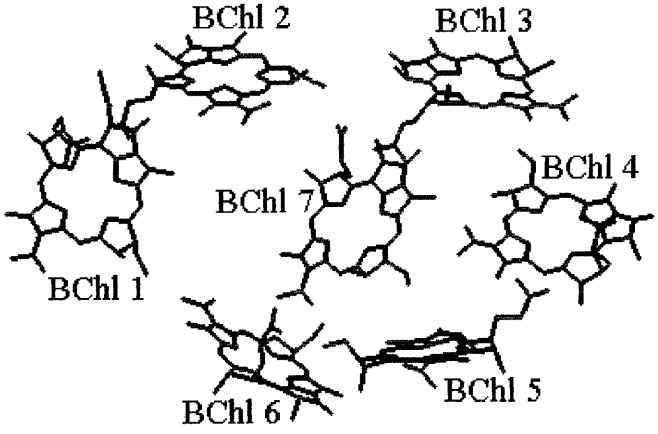

Fig. 1 A 2-D view of the bacteriochlorophylls (BChls) of the monomeric subunit of the trimeric Fenna-Matthews-Olson (FMO) complex of *Prosthecochloris aestuarii*. BChls are labeled in the Fenna and Matthews (1975) numbering scheme

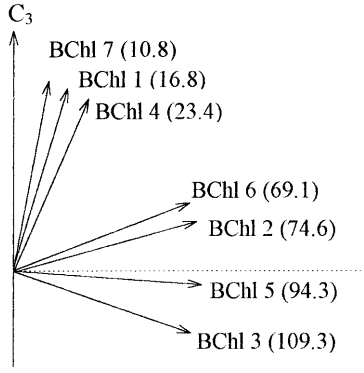

Fig. 2 Individual Q_y transition dipole moment directions of the monomeric BChls with respect to the C_3 symmetry axis. The *dashed line* corresponds to the direction of the macroscopically defined axis in the linear dichroism measurements. The *numbers in parentheses* are the values of the angles that the dipole moments make with the C_3 symmetry axis

EES models for FMO have generally been based on obtaining an optimal match between the information contents of the optical steady-state spectra and the molecular organization (Pearlstein 1991, 1992; Lu and Pearlstein 1993; Gülen 1996; Iseri and Gülen 1997; Louwe et al. 1997a). Recent spectral and kinetic information gathered from probing the excited state processes through ultrafast measurements (Savikhin and Struve 1994, 1996; Buck et al. 1996; Freiberg et al. 1997; Savikhin et al. 1997; Vulto et al. 1997) have not yet been used effectively for further refinement of the EES and for quantification of the relation between the EES and the excited state kinetics.

We have incorporated the temporal and spectral information provided by the low-temperature absorption difference spectra (ADS) reported recently (Vulto et al. 1997) into the model calculations on the EES of the FMO in addition to several steady-state spectra. We have discussed the implications of the proposed EES for equilibration of excitation energy in the excited state manifold at low temperatures.

Review

The 3-D structure of the FMO complex of the green bacterium *P. aestuarii* reveals three identical subunits related by a crystallographic threefold axis of symmetry (C_3). Each subunit encloses seven BChl molecules arranged in a rather non-symmetric fashion (see Fig. 1). The BChls are confined within an ellipsoid of axial dimensions: 45 Å×35 Å×15 Å. The average center to center distance between BChls is 12 Å in the same subunit and the closest BChl–BChl distance between different subunits is 24 Å. At distances around 10–20 Å it is expected that the delocalized states (excitons) that result from the dipole-dipole interactions among the BChls are the electronic states responsible for energy transfer and the optical characteristics are mainly determined by such excited states.

Two essential factors controlling the delocalization characteristics of the EESs are the site energies and the protein refractive index. For the LHCs, convincingly accurate determinations of these parameters are not yet possible starting from first principles. It has recently been discussed that the measurements which can give information about the dipole moment directions of the electronic transitions of the FMO complex with respect to the C_3 symmetry axis and their subsequent modeling can be particularly useful in suggesting empirical values for these two key factors (Gülen 1996; Iseri and Gülen 1997; Louwe et al. 1997a, b), owing to a very specific dipole moment organization of the BChls. This specific organization which proved to be very useful in correlating the spectra with the structure is shown in Fig. 2; the directions for the BChls 1, 4, and 7 are approximately parallel to the C_3 symmetry axis while the directions for the BChls 2, 3, 5, and 6 are very much in the plane of the trimer.

In the recent EES models (Pearlstein 1992; Lu and Pearlstein 1993; Gülen 1996; Iseri and Gülen 1997; Louwe et al. 1997a) it is agreed that each BChl can experience a different site energy due to different protein environments and different conformational properties. Furthermore, it is also accepted that one of the BChls is relatively red-shifted from the others. However, there exist several contrasting hypotheses on the identity of the red-most BChl. Best fits to the absorption (ABS) and circular dichroism (CD) spectra of Olson et al. (1976) predict that the red-most pigment is BChl 7 (Pearlstein 1992; Lu and Pearlstein 1993). Best fits to the ABS and CD spectra of Phillipson and Sauer (1972), on the other hand, suggest BChl 3 as the red-most pigment (Lu and Pearlstein 1993). Best fits to the ABS, linear dichroism (LD), and singlet-triplet absorption difference (STAD) spectra of van Mourik et al. (1994) suggest the red-most pigment as BChl 6 (Gülen 1996). On the basis of the simultaneous simulation of the ABS and LD spectra, it has been suggested that the red-most pigment should be either one of BChl 6 or BChl 3 (Iseri and Gülen 1997). Most recently, Louwe et al. (1997a) have suggested

a model in which the red-most pigment is BChl 3 by simultaneously simulating their own ABS, linear dichroic-STAD, and STAD data, the LD spectrum of van Mourik et al. (1994), and the CD spectrum of Vasmel et al. (1983).

The model by Louwe et al. (1997a) is based on exciton calculations with substantially lower dipolar interactions than used in the other models mentioned above (a factor of 1.30–1.35 reduction in the dipole moment strengths is proposed). It has been discussed that the simulations improve substantially at lower dipolar interactions. At lower dipole moment strengths, the properties of the individual BChl dipole moments gain growing importance in controlling the delocalization characteristics of the EESs.

Except for the model of Louwe et al. (1997a), all the models mentioned above are obtained using the trimeric FMO based on the identification of two distinct red-most transitions (around 825 nm) in a hole-burning study on *P. aestuarii* (Johnson and Small 1991). More recently, two groups have provided convincing evidence that the excitation is localized in one of the subunits. It has been discussed that the results of the pump-probe anisotropy decay experiments on the FMO complex of *Chlorobium tepidum* cannot be explained with the trimeric exciton models. Anisotropy data can be simulated more consistently if the excitation energy is mainly localized within a subunit of the trimer (Savikhin et al. 1997). Recent observations on the character of the triplet state (linear-dichroic absorbance-detected magnetic resonance measurements on the FMO complex of *P. aestuarii*) have also been discussed to be consistent if the triplet state associated with the red-most band is localized within a single subunit and if it is almost entirely associated with one of the BChls (Louwe et al. 1997b).

Summarizing, in all the models mentioned above a match between the information contents of the steady-state spectra and the molecular organization has been sought. There exists no modeling study which has used the wealth of temporal and spectral information offered by the ADS measurements on the FMO complex (Savikhin and Struve 1994, 1996; Buck et al. 1996; Freiberg et al. 1997; Savikhin et al. 1997; Vulto et al. 1997) with the purpose of further refinement of the EES structure.

Recently, ADS simulations have been reported for two of the models (Lu and Pearlstein 1993) by Buck et al. (1996). Important messages communicated in this study were: simulation of the ADS is another effective source of information; different models that can be rated equally acceptable in interpretation of steady-state spectra can yield broadly dissimilar simulations of the ADS; therefore, ADS simulations should be useful in distinguishing between different models and should be integrated as an important element of refinement in the further modeling studies. In this particular study, simulations obtained with *P. aestuarii* structure (Tronrud et al 1986) have been compared to the transient absorption data (ADS) of *C. tepidum* (Buck et al. 1996). At that time, neither the structural data of *C. tepidum* nor the ADS data of *P. aestuarii* were available (all the other ADS studies mentioned above had been on *P. aestuarii*). Both have been available very recently (Li et al. 1997; Vulto et al. 1997). Therefore, further refinement is now plausible by modeling the spectral and temporal characteristics of ADS in addition to the optical steady-state spectra.

Theory

The file containing the atomic coordinates (Tronrud et al. 1986) of the FMO complex of *P. aestuarii* has been imported from the Protein Data Bank, Brookhaven.

The dipole-dipole interaction between a pair of BChls has been calculated in the point dipole approximation. For each BChl, the direction of the transition dipole moment associated with the singly excited Q_y transition has been taken to be parallel to the axis passing through the N_B-N_D nitrogen atoms in the nomenclature of the Protein Data Bank file (i.e., corresponding to N_{21} and N_{23} according to IUPAC nomenclature).

ABS, LD, and STAD spectra have been simulated as described by Pearlstein (1991) on the basis of one-exciton states. ADS has been simulated as described by Buck et al. (1996) on the basis of two-exciton states. The time evolution of the ADS is found using the Pauli master equation formalism (Knox 1975). The rate of energy transfer between a pair of BChls has been calculated using an approximation (Jean et al. 1988) to the Förster formula (Förster 1965). The effective energy transfer rate between two non-extensively delocalized one-exciton states is approximated as a linear combination of the Förster rates between the BChl pairs dominating the Q_y occupancies of such states. Details of the calculations can be found in Iseri (1998).

The 4 K experimental ABS, LD, and STAD spectra (see Figs. 3 or 4) have been taken form van Mourik et al. (1994) The time-resolved ADS data (10 K) shown in Fig. 5 have been taken from Vulto et al. (1997).

Results and discussion

Steady-state spectra simulations

In our previous work (Gülen 1996; Iseri and Gülen 1997) we have already discussed the problems associated with the models suggested by Lu and Pearlstein 1993) which offered optimal fits to the ABS and CD spectra of Olson et al. (1976) and Phillipson and Sauer (1972). It has been noted that none of these models can give acceptable fits to the LD and STAD data of van Mourik et al. (1994). It has also been noted that some of the linewidths used in these simulations (185–350 cm^{-1}) are far broader than inferred by hole-burning measurements (70–80 cm^{-1}) (Johnson and Small 1991). It was therefore clear that, if the site energy sets of these models are used to simulate ABS and CD with a common linewidth around 80 cm^{-1}, substantial deviations from the experimental data occur.

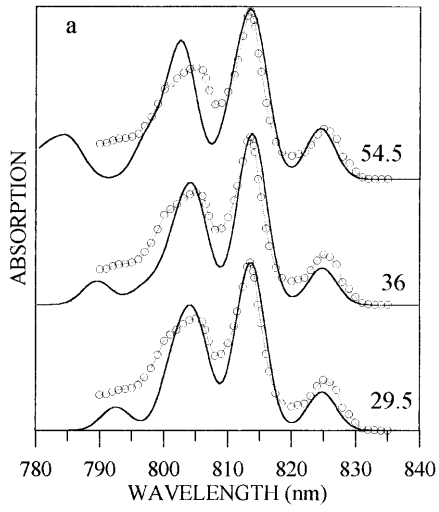

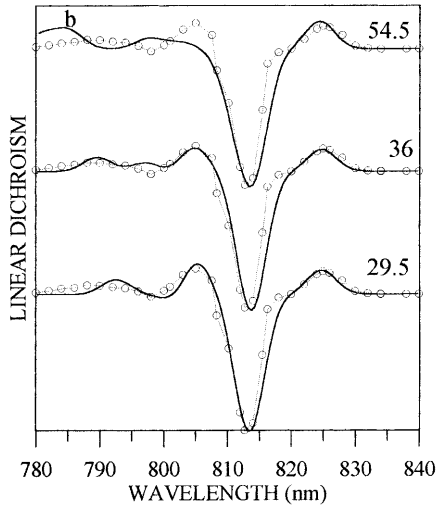

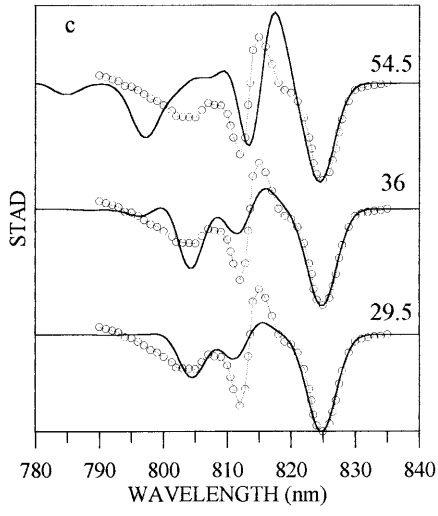

Fig. 3 Comparison of the simulated absorption (ABS; **a**), linear dichroism (LD; **b**), and singlet triplet absorption difference (STAD; **c**) spectra (*solid lines*) to the experimental data (*open dots*) for the BChl 3 model. Simulations are carried out at the three different absorption strengths (in D^2) indicated. Simulated ABS and LD spectra are normalized to the peak absorbing at 813 nm, and the simulated STAD spectra are normalized to the peak at 825 nm

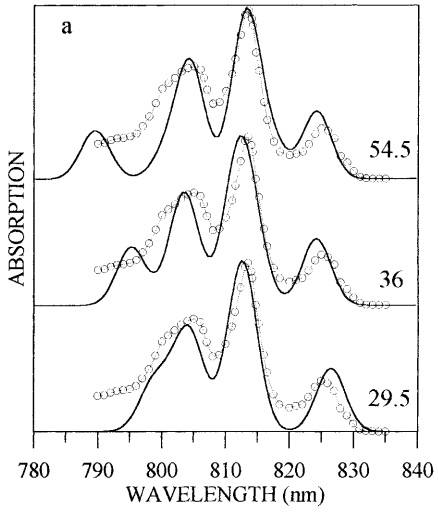

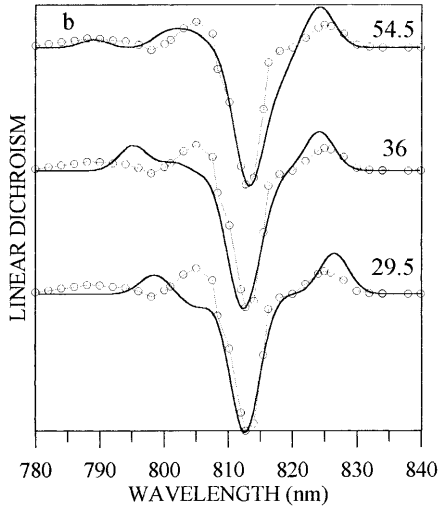

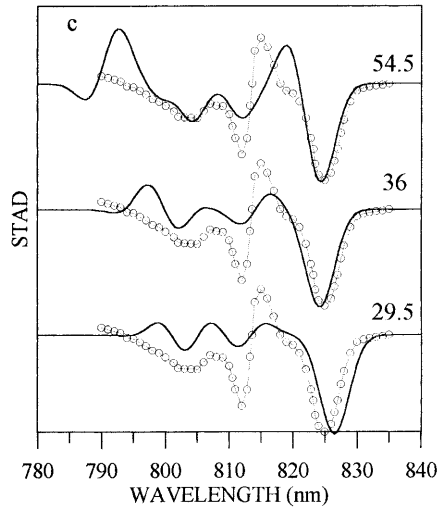

Fig. 4 Comparison of the simulated ABS (**a**), LD (**b**), and STAD (**c**) spectra (*solid lines*) to the experimental data (*open dots*) for the BChl 6 model. Simulations are carried out at the three different absorption strengths (in D^2) indicated. Simulated ABS and LD spectra are normalized to the peak absorbing at 813 nm, and simulated STAD spectra are normalized to the peak at 825 nm

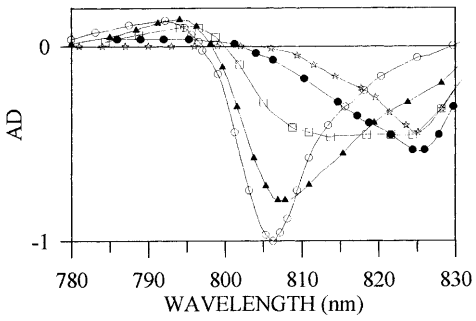

Fig. 5 Low-temperature (10 K) absorption difference spectra (ADS) of *P. aestuarii* at specific time delays for excitation at 806 nm reported by Vulto et al. (1997). The delays between the pump and probe pulses are: 0.1 (*open dots*), 0.5 (*triangles*), 1.7 (*squares*), 5.5 (*dots*), and 25 (*stars*) ps

We have also provided examples demonstrating that it is adequate to associate one of BChls 2, 3, 5, and 6 with the red-most (825 nm) band while the BChls 1, 4, and 7 should be associated with the transition(s) around 815 nm in order to explain the key features of the LD spectra in the Q_y region. Furthermore, based on the optimal fits to the ABS and LD data of van Mourik et al. (1994), we have concluded that the models in which either BChl 3 or BChl 6 is the red-most pigment are more likely to reproduce the steady-state absorption characteristics, while the models in which BChl 2 or BChl 5 is the red-most pigment have been disfavored (Iseri and Gülen 1997). On the other hand, based on the optimal fits of ABS, LD, and STAD spectra, we have suggested a model in which BChl 6 is the red-most pigment (Gülen 1996). In our previous models, simulations have been carried out for the trimeric FMO. The absorption strength of each BChl was 54.5 D^2 and each one-exciton transition was dressed with a symmetric Gaussian of linewidth 80 cm^{-1}.

Following the recent developments, we have reanalyzed the optical steady-state spectra mentioned above. The major assumptions used for modeling the steady-state spectra are listed below.

1. It is assumed that each BChl can experience a different site energy due to different protein environments and different conformational properties but dynamical disorder is neglected. One of the BChls 2, 3, 5, and 6 is assumed to be the red-most pigment.
2. Simulations are carried out for the monomeric subunit of the C_3 trimer.
3. The absorption strength of each BChl, assumed equal for all BChls, is let as a free parameter and is varied between 25 and 55 D^2 following the values in the literature.
4. A common symmetric Gaussian of linewidth 80 cm^{-1} is used for dressing each one-exciton transition.

In the recent model by Louwe et al. (1997a) a similar set of assumptions has already been used. We, however, have reconsidered the simulations for several reasons. First of all, the data used in their model display an overall red shift (around 2–3 nm) in the positions of the absorption bands compared to all other low-temperature data existing in the literature. Moreover, we intend to search for a model that not only can explain steady-state spectra but also time-resolved data. It was therefore rational to regard the absorption strength and the site energies as free parameters yet to be adjusted, instead of accepting a very specific set of values reported by Louwe et al. (1997a). Furthermore, we also would like to note that if the CD is excluded it is rather difficult to distinguish between the BChl 3 and the BChl 6 models using the simulations provided in this particular study. In addition, CD simulations are very sensitive to minor changes in the atomic structure (Gülen 1996), to the dynamical disorder in site energies (Buck et al. 1997), and currently available CD data (Phillipson and Sauer 1972; Olson et al. 1976; Vasmel et al. 1983) display sizable differences.

The general strategy followed for selection of a suitable initial set of BChl site energies has already been discussed in detail (Gülen 1996; Iseri and Gülen 1997). We briefly summarize several points that have been critical in this respect.

- Unless at least one of the BChls is relatively red shifted from the others, the absorption band around 825 nm cannot be reproduced (e.g. see Fig. 3a). It has an integrated absorption strength of around 1 BChl per monomer. It can therefore be assumed that the 825 nm band is dominated by one of the BChls.
- The LD spectrum (e.g. see Fig. 3b) has the following distinctive features: a positive LD band around 825 nm, a strongly negative LD band around 815 nm, a positive LD signal around 805 nm, and almost vanishing LD activity on the blue-most side of the spectrum. The prevailing contribution to the strongly negative 815-nm LD band should be from the BChls whose dipole moments are more or less parallel to the C_3 symmetry axis (or perpendicular to the macroscopic alignment axis, i.e., BChls 1, 4, and 7). One of BChls 2, 3, 5, and 6 whose dipole moment directions are almost perpendicular to the C_3 symmetry axis should predominantly account for the 825-nm positive LD signal. Once one of BChls 2, 3, 5, or 6 is fixed to be the red-most pigment, the remaining three BChls should be contributing mostly to the bands around 800–805 nm.
- Further initial fine tuning of the site energies can be achieved by taking into account the shift tendencies (blue or red) of the important pairwise interactions in the Hamiltonian. In the Hamiltonian the strongest interactions are between the nearest neighbors (BChl 1-BChl 2, BChl 2-BChl 3, etc.). The BChl 4-BChl 7 interaction is the only exception.

New initial site energy sets are created at several different absorption strengths in the 25–55 D^2 range following the strategy described above. Further adjustment is done around these sets manually in an interactive fit routine [e.g. see Louwe et al. (1997a) for the problems associated with the automatic search routines].

We have first asked which of the BChls 2, 3, 5, and 6 is most likely to be the red-most pigment based on simulta-

neous fits of the ABS and LD data. The same conclusion has again been arrived at: either BChl 3 or BChl 6 should be the red-most pigment; BChl 2 and BChl 5 cannot explain the prominent spectral signatures of the ABS and LD simultaneously. We do not show any simulations for the BChl 2 and BChl 5 models and we refer to Figs. 3 and 4 for the BChl 3 and BChl 6 models, respectively. Briefly, the main problems encountered for these cases in the absorption strength range given above were: in the optimal BChl 2 ABS + LD fits, the red-most LD signal could only be generated with almost vanishing positive intensity; and similarly in the optimal ABS + LD fits for BChl 5, the 805 nm band could not gain enough absorption strength. Therefore, from this point on, the discussion is restricted to the BChl 3 and BChl 6 models.

At this stage our intention is not to obtain the best fits, but to observe the systematic changes occurring in the spectral features as a function of the absorption strength in order to decide the absorption strength range which is likely to explain the key features of the steady-state spectra. It should be emphasized that exciton calculations contain a number of approximations and simplifications. Among those, we have uncertainties in the interactions between the molecules. Use of more precise BChl wavefunctions is necessary for a better evaluation of the interactions (Pearlstein 1991). Very recent ab initio calculations of Coulombic interactions between the transition densities of several BChl pairs in the LH2 complex of purple bacteria (*Rhodopseudomonas acidophila*) suggest that the Q_y transitions of BChl molecules are reasonably well described by the point dipole approximation for separations greater than 15 Å and deviations are significant at separations around 9–9.5 Å (Krueger et al. 1998). In the FMO complex there are no BChl pairs closer than 11 Å. Most of the leading interactions are due to BChls at separations greater than 13 Å. Several pairwise interactions (1–2, 3–4, and 5–6) are most likely to be subjected changes. In the LH2 complex there are no pairs at comparable distances (11–13 Å) and the extent of deviations from the point dipole approximation remains to be investigated. Furthermore, the effect of dynamical disorder in the protein environment is neglected (Buck et al. 1997). However, we believe that inclusion of disorder is only necessary for additional fine tuning. Preliminary calculations (Louwe et al. 1997a) indicate that for a single subunit of the FMO complex, inclusion of disorder does not noticeably change the results of a particular simulation of the optical spectra. In view of these approximations and simplifications, we have restricted the calculations to a minimal set of free parameters and our objective has been simultaneous reproduction of only the prominent spectral signatures.

ABS, LD, and STAD simulations for three different absorption strengths are compared to the experimental data in Figs. 3 and 4. The corresponding site energy sets are listed in Table 1. Examination of the simulations indicates that optimal ABS + LD fits yield little basis for differentiation between the BChl 3 and BChl 6 models. (In the figures presented we have simultaneously simulated ABS + LD + STAD spectra. If only ABS + LD are simulated, better fits can be obtained in the absorption strength range studied.)

Table 1 BChl site energies (in nm) used in the simulations of Figs. 3 and 4

BChl	BChl 3 model			BChl 6 model		
	Absorption strength (D^2)			Absorption strength (D^2)		
	29.5	36	54.5	29.5	36	54.5
1	809.4	808.0	805.2	806.8	806.2	801.0
2	805.2	802.1	790.8	805.7	801.0	802.1
3	823.4	822.8	820.6	803.1	803.1	805.2
4	810.5	809.4	804.7	808.3	807.8	806.8
5	797.9	795.9	799.5	806.8	804.2	801.0
6	801.0	800.5	789.8	824.5	821.2	817.4
7	803.1	804.2	804.2	804.2	804.2	805.2

For the BChl 3 model, considerably better agreement between the simulations and the experimental data is obtained at lower absorption strengths. Two major discrepancies, the large negative STAD signal at 795 nm and the overall disagreement with the LD spectrum on the blue side of the spectrum, tend to disappear as the strength of the excitonic interactions are reduced. At lower absorption strengths, ABS and LD fits are better. In the STAD simulations, the relative strengths of the 805 nm and 812 nm bands do not agree with the experiment.

For the BChl 6 ($\mu^2 = 54.5\ D^2$) model, except the positive 795 nm STAD signal, the key features of all three spectra are mainly reproduced. The agreement between the simulations and the experiments is considerably less satisfactory at lower absorption strengths.

Summarizing, through simultaneous simulations of ABS, LD, and STAD in the absorption strength range 25–55 D^2, we have concluded that the BChl 3 models with $\mu^2 \cong 30-40\ D^2$ and BChl 6 models with $\mu^2 \cong 45-55\ D^2$ can satisfactorily explain the key features of all three optical spectra.

Absorption difference spectra simulations

At a certain probe pulse delay (t), the absorption difference spectrum contains contributions from the photobleaching (PB) of the ground state (transitions from the ground state to one-exciton states ≡ EESs), stimulated emission (SE) from the one-exciton states, and absorption from the one-exciton states to two-exciton states (excited state absorption, ESA). Refer to van Amerongen and van Grondelle (1995) for a detailed account of the experimental technique and to Buck et al. (1996) for a detailed description of theoretical calculations.

The PB spectrum is independent of the excitation wavelength because all one-exciton transitions arise from a common ground state, i.e., the entire one-exciton spectrum is uniformly bleached at any excitation wavelength. However, the prompt ESA and SE occur only from the laser-populated one-exciton states. The integrated spectra for BP and SE between a pair of ground and excited electronic

states are equal. Under the technical conditions of the current ADS measurements the PB spectrum is considered constant in time. Therefore, the time evolution of ADS at a certain wavelength (λ) at times much shorter than the excited state lifetime (around nanoseconds for BChl) is governed by the changing contributions of SE and ESA spectra to the ADS in the course of relaxation of electronic energy in the excited state manifold: $\mathrm{ADS}(\lambda, t) \equiv \mathrm{ESA}(\lambda, t) - \mathrm{PB}(\lambda, t) - \mathrm{SE}(\lambda, t)$.

Figure 5 shows time-resolved ADS of the FMO complex from *P. aestuarii* (Vulto et al. 1997). Data have been taken with excitation at 806 nm (pulse width ≈100 fs) at low temperature (10 K). Low-temperature ADS at different time delays are highly structured and a complex evolution in spectral intensities is observed. Shortly after excitation (at 0.1 ps), ADS exhibits two main features: an ESA band on the blue side of the spectrum (peaking around 792 nm) and a strong PB/SE band around 806 nm. At later times, two effects are dominant. First of all, the intensity of the 792 nm ESA band decreases gradually and at the same time its peak is shifted toward longer wavelengths. It almost vanishes after 5.5 ps. Secondly, the strong 806 nm PB/SE signal progressively loses strength in favor of the 815 nm and 825 nm bands. This redistribution indicates ultrafast loss of the initial excited state population and a simultaneous population gain of the lower energy levels. Population gain in all the lower energy bands (810 nm, 815 nm, and 825 nm) is apparent as early as 0.5 ps. At 1.7 ps delay, the absorption intensity around 806 nm is reduced to less than half of its initial value, while the 810–815 nm and 825 nm bands are bleached further. Around 5.5 ps, bleaching of the 825 nm band is maximal while the bleaching around 815 nm has decreased considerably. After 5.5 ps, the only process detected is the decay of 825 nm band. Full spectral equilibration is observed to take place in about 40 ps.

We have simulated the PB, SE, and ESA contributions to the absorption difference using the formalism described by Buck et al. (1996). To facilitate a comparison with the experimentally observed time evolution of the ADS, we have first generated the ADS corresponding to each EES. In generating the ADS of each EES, a symmetric Gaussian of linewidth 140 cm^{-1} (note that this is different from the 80 cm^{-1} width used in steady-state spectra simulations – in pump-probe experiments bandwidths are usually broader due to experimental artifacts) is used to dress each spectral component in the ground to one-exciton PB transitions, in the one-exciton to two-exciton ESA transitions, and in the SE transitions. The positions of the SE and PB bands are assumed equal [we have neglected the Stokes shifts – for the FMO believed to be small at around 40 cm^{-1} – e.g., see van Amerongen and Struve (1991)] and the ESA of the monomeric BChl is neglected. Then, ADSs at different time delays of the probe pulse have been simulated by using the ADS of each EES in a relaxation scheme consistent with the experimentally observed kinetics. For comparisons with the data shown in Fig. 5, the initial state has been taken as the prompt (unrelaxed) ADS at 806 nm.

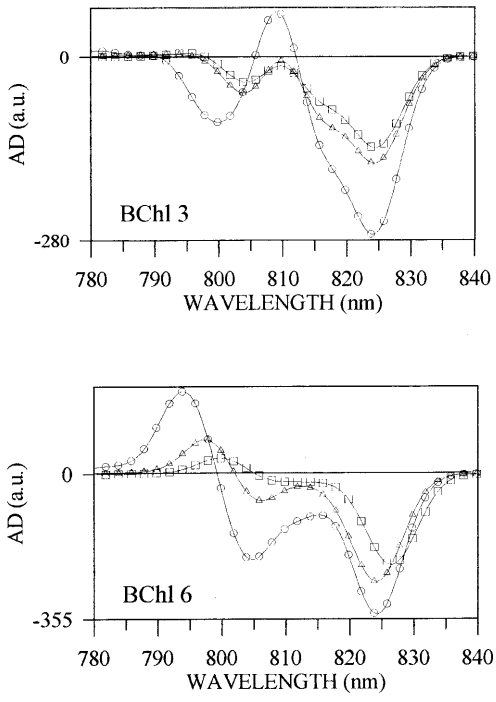

Fig. 6 Prompt ADS simulations at 825 nm excitation for the BChl 3 and the BChl 6 models at three different absorption strengths. In both panels the absorption strengths are: 54.5 D^2 (*dots*), 36 D^2 (*triangles*), and 29.5 D^2 (*squares*). At 825 nm excitation the lowest electronic excited state (EES) is almost selectively excited

As discussed above, in *P. aestuarii* at 10 K, downhill excitation relaxation to the lowest EES is almost complete within 5–10 ps (at 10 K the uphill transfer can be neglected). Therefore, the prompt ADS simulated with excitation pulses centered around the lowest EES (≈825 nm) should, to a large extent, resemble the experimental ADS at delay times of around 5–10 ps.

Prompt ADS simulations at 825 nm excitation obtained using the parameter sets for the BChl 3 and BChl 6 models (see Table 1) are shown in Fig. 6. Simulations are to be compared to the experimental ADS at $t = 5.5$ ps delay, presented in Fig. 5.

For the BChl 6 model, prompt ADS simulations in the absorption strength range that is found to give satisfactory fits to the steady state spectra (≅45–55 D^2) display significant discrepancies with the experiment. In this range, relative PB/SE contributions of the 805 nm and 825 nm bands are in apparent disagreement with the experiment. Moreover, the simulated ADS have a strong ESA band on the blue side of the spectrum. In the absorption strength range 30–40 D^2, the resemblance between the simulated and observed ADS is closer. However, in this range, steady-state spectra cannot be simulated satisfactorily (see Fig. 4).

Similarly, for the higher absorption strength (≅45–55 D^2) BChl 3 simulations, the relative contributions of the 805 nm and 825 nm PB/SE signals are inconsistent with the ADS data. In addition, the ESA contribution around 810 nm is absent in the experiments. In the absorption strength range (≅30–40 D^2) in which steady-state spectra can be satisfac-

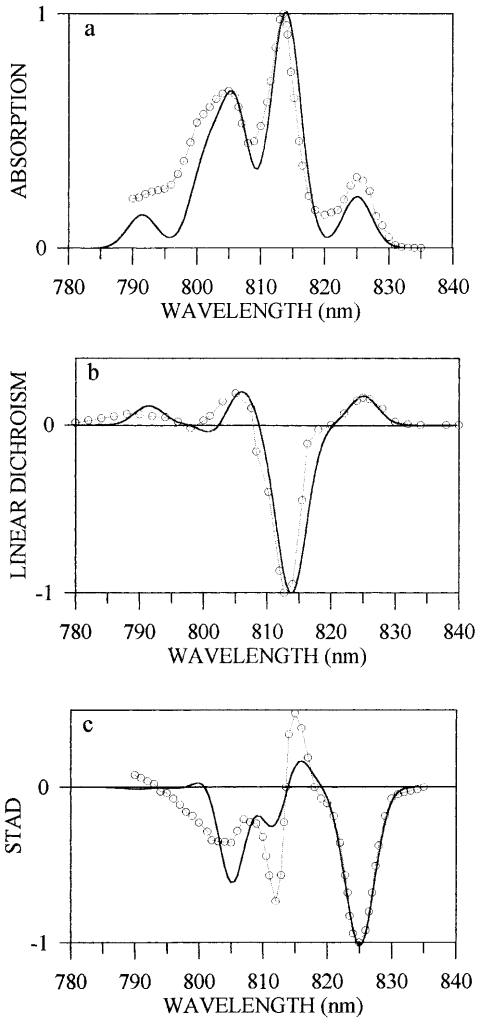

Fig. 7 ABS (**a**), LD (**b**), and STAD (**c**) simulations at $\mu^2 = 32.6$ D^2 in comparison with the experimental data. Simulations (*solid lines*) and experimental data (*open dots*). The site energies (in nm) are: BChl 1 (808.87), BChl 2 (805.19), BChl 3 (823.37), BChl 4 (810.45), BChl 5 (796.91), BChl 6 (802.06), BChl 7 (803.10). The EESs are (in nm) at: 791.47, 799.63, 801.52, 805.85, 812.78, 814.07, and 825.04. Simulated ABS and LD spectra are normalized to the peak absorbing at 813 nm and simulated STAD spectra are normalized to the peak at 825 nm

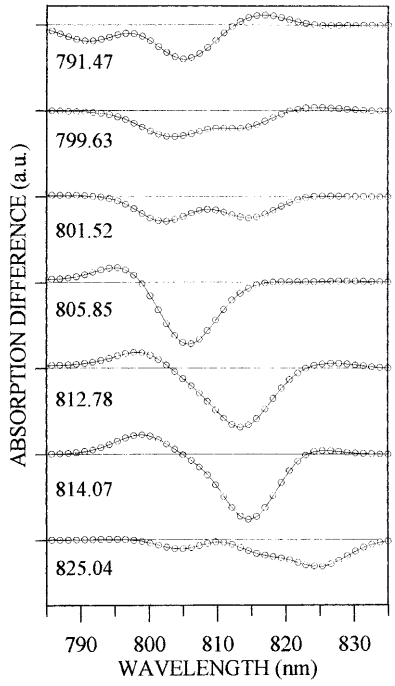

Fig. 8 ADS for each EES at $\mu^2 = 32.6$ D^2. All the ADS curves are drawn on the same absolute scale. The transition energy of each EES is indicated (in nm)

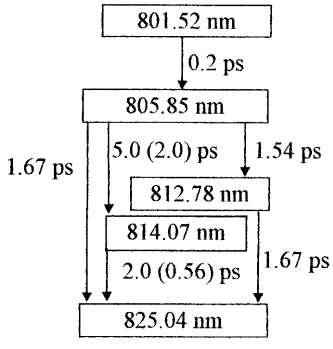

Fig. 9 Kinetic models [model a and model b (with the rates in parenthesis)] used in describing the time evolution of the ADS. In both models the lowest EES decays with a time constant of around 40 ps

torily reproduced (see Fig. 3), all prominent ADS features over the entire Q_y band are generated as well. In particular, the PB/SE behavior at wavelengths longer than 800 nm is reproduced and the ESA on the blue vanishes as observed in the pump-probe experiments.

We have therefore considered only the BChl 3 model for further simulations including the time evolution of ADS. Optimization of ABS, LD, STAD, and ADS at five different time delays is sought in the absorption strength range 30–40 D^2. As discussed above, it is difficult to favor a particular absorption strength value in this range on the basis of simultaneous ABS, LD, and STAD simulations. Similarly, a satisfactory time evolution can be obtained within the minor variations of the proposed kinetic scheme(s) in this absorption strength range. For illustrative purposes, we have arbitrarily selected $\mu^2 = 32.6$ D^2 and have presented the typical results for this case. The optimized ABS, LD, and STAD simulations are given in Fig. 7. The ADS corresponding to each EES are illustrated in Fig. 8. Typical schemes representing the type of kinetic models that are decided to produce an optimal match with the experimental ADS is given in Fig. 9. Simulated ADS for the delay times of 0.1, 0.5, 1.7, 5.5, and 25 ps are shown in Fig. 10.

At 806 nm, the 801 nm, 806 nm, and 812 nm bands are excited with the respective probabilities of 27%, 57%, and 10%. Downhill energy transfers show a multiexponential character. Relaxation between the 801 and 806 levels is ultrafast (200 fs). The 806 nm level relaxes into 812, 814, and 825 nm levels with 1.54, 5, and 1.67 ps kinetics, re-

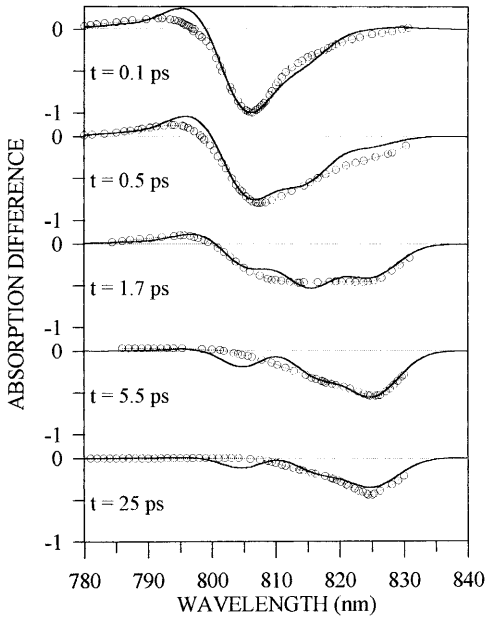

Fig. 10 Comparison of the experimental (*open dots*) and the simulated (*solid lines*) ADS of *P. aestuarii* at five different delay times upon excitation at 806 nm for the BChl 3 model with $\mu^2 = 32.6$ D^2 for model a of Fig. 9

spectively (model a of Fig. 9). The 825 nm level is also populated by the 812 nm and 814 nm levels with respective kinetics of 1.67 ps and 2.0 ps (model a of Fig. 9). Lifetime of the 825 nm level is around 40 ps. In the second scheme (model b of Fig. 9), which yields ADS almost identical to those presented in Fig. 10, excitation relaxes through the same channels, but the relaxation rates in the 806 nm → 814 nm → 825 nm transfer pathway are both faster (814 nm → 825 nm transfer is 0.67 ps and 806 nm → 825 nm is 2.0 ps). In the selected absorption strength range, the time evolution can be reproduced using slightly different versions of these kinetic schemes with minor changes in the rates.

Upon examination of the ADS corresponding to each EES shown in Fig. 8, it is already clear that the evolution of the four major spectral bands can be understood by the downhill (806 nm → 812–815 nm → 825 nm) relaxation of the electronic excitation energy. The multi-exponential kinetic models offer further fine tuning of the evolution of the ADS. Both the spectral and the time evolution of the blue ESA band is reproduced. Although the fits are not perfect, they are satisfactory. The EESs at 806, 812, and 815 nm are the main contributors to this ESA signal. Upon 806 nm excitation, the progressive red shift in the peak position and the accompanying decay is due to the downhill relaxation of the energy to the lower EESs. Except the 791 nm state, for all the EESs the PB/SE contributions overcome the ESA contributions at wavelengths longer than 800–805 nm. The ADS corresponding to the 825 nm level has a predominant PB/SE contribution on the red edge; however, a weak PB/SE signal around 805 nm still persists. This weak PB/SE signal is the origin of the slight discrepancy between the simulations and the experiments at delay times longer than several picoseconds.

To get a clear physical interpretation of the observed kinetics, independent theoretical estimates of the relaxation rates are essential. Two limiting behaviors – very weak and strong coupling limits – are usually identified by the relative magnitudes of a number of energies. These energies are: the interaction energy, the absorption linewidth (homogeneous broadening), and the dispersion in the site energies (inhomogeneous broadening). When the magnitude of the interaction energy is overpowered by the homogeneous and inhomogeneous broadenings, the very weak coupling limit applies; the EESs are localized and excitation transfer is described by the Förster transfers between the pairs of molecules. In the strong coupling limit, excitation transfer is described by the relaxations between the eigenstates of the system whose degrees of delocalization are mainly decided by the magnitude of the electronic interaction energy (Förster 1965).

For the FMO complex, all three energies are of comparable magnitude and, generally speaking, the system is in the "intermediate" coupling regime. The site energy shifts (estimated to correspond to a distribution of about 80–100 cm^{-1} halfwidth) are comparable with the absorption linewidths of the EESs in the steady-state absorption spectrum (80 cm^{-1}). Similarly, the magnitude of the dipole-dipole interactions between several leading BChl pairs (around 65–110 cm^{-1} for $\mu^2 = 30$–40 D^2) is comparable with the widths of the other two.

To give an idea about the delocalization characteristics of the EESs in the absorption strength range selected $\mu^2 \cong 30$–40 D^2), the contributions of each BChl to the occupation probability of each EES for $\mu^2 = 32.6$ D^2 are listed in Table 2. In each EES at least about 50% of the excitation is localized on a particular BChl following the trends

Table 2 Contributions of each BChl to the occupation probability of each EES at $\mu^2 = 32.6$ D^2

Site energy (nm)	EES energy (nm)	Occupation probability on BChl						
		1	2	3	4	5	6	7
796.9 (BChl 5)	791.47	0.001	0.003	0.001	0.073	**0.616**	0.272	0.035
805.2 (BChl 2)	799.63	0.319	**0.520**	0.003	0.000	0.051	0.016	0.091
803.1 (BChl 7)	801.52	0.037	0.093	0.001	0.090	0.093	0.002	**0.683**
802.6 (BChl 6)	805.85	0.001	0.028	0.018	0.132	0.140	**0.667**	0.013
810.5 (BChl 4)	812.78	0.090	0.052	0.094	**0.490**	0.091	0.042	0.141
808.9 (BChl 1)	814.07	**0.547**	0.286	0.000	0.126	0.007	0.000	0.034
823.4 (BChl 3)	825.04	0.005	0.019	**0.882**	0.088	0.002	0.001	0.002

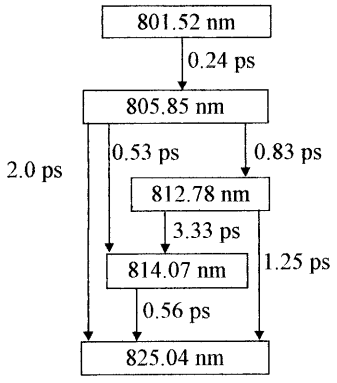

Fig. 11 Kinetic model resulting from the effective transfer rate estimations

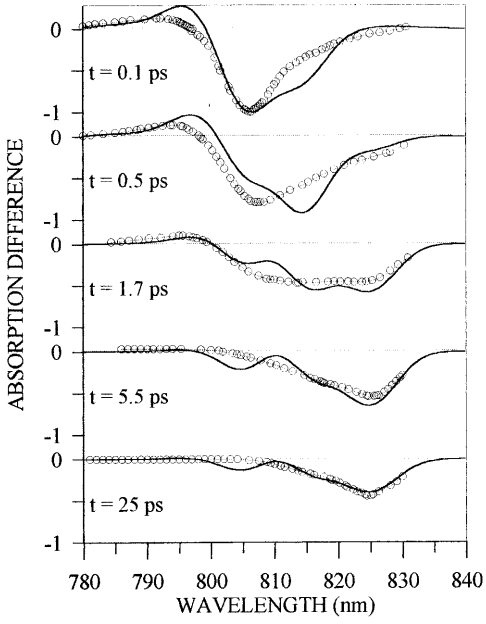

Fig. 12 Comparison of the experimental (*open dots*) and the simulated (*solid lines*) ADS of *P. aestuarii* at five different delay times upon excitation at 806 nm for the BChl 3 model with $\mu^2 = 32.6\ D^2$ for the kinetic model of Fig. 11

in the site energy shifts and the shift tendencies of the leading electronic interactions. The lowest energy state is almost localized on BChl 3. All the other states are non-extensively delocalized: excitation is effectively localized on two or three BChls.

In an intermediately coupled system, downhill rates are expected to include contributions from both the Förster and the exciton relaxation rates (Knox and Gülen 1993). Nevertheless, to get a preliminary view on the connection between the EES structure and the excited state dynamics, we have provided zero-order estimates of the rates for the energy transfer pathways resulting from the EES model. We have calculated the effective transfer rates between two non-extensively delocalized EESs as a linear combination of the Förster rates between the BChls dominating the occupation probabilities of such states. The estimated effective rates are indicated in the kinetic scheme of Fig. 11. There is a good agreement between the values of the estimated rates and the empirical rates found by fitting the time evolution of the ADS as long as the time scales are concerned. The biggest inconsistency is in the depopulation of the 806 nm level. It can therefore be said that most of the essential spectral and temporal features in the time evolution of the ADS are described by the estimated effective rates which are found by using the Förster formula. To furnish a more direct judgement we have illustrated (see Fig. 12) the time evolution of the ADS simulated by using the effective transfer rates of Fig. 11 instead of the rates provided in Fig. 9.

We stress that the actual physical description of the excitation dynamics can only be provided by following the dynamics using a transport tool appropriate in the intermediate coupling limit (Kenkre and Knox 1974; Knox and Gülen 1993; Struve 1995; Leegwater et al. 1997). To gain more insight into the nature of energy transfer in the FMO complex, analysis of the time evolution of further isotropic and anisotropic pump-probe experiments using such transport tools are necessary.

We also would like to comment on the portability of our results to the FMO complex of *C. tepidum*. A recent structural model of *C. tepidum* (Li et al. 1997) shows that the overall structures of the two FMO complexes (*C. tepidum* and *P. aestuarii*) are very similar. The two complexes have been compared in detail in terms of several different structural properties that may cause differences in the BChl interactions and BChl site energies, such as the protein environments, the ligand bindings, the H-bondings, and the conformations of the tetrapyrroles and phytyl chains of the BChls (Li et al. 1997). The most significant differences are observed in the planarity of several BChls and it has been noted that the BChls 2 and 6 are most different. It has long been known that the low-temperature ABS and CD spectra of the FMO complexes from these two different species show differences in the wavelength positions and relative amplitudes of the spectral bands (Olson et al. 1976). Very recently the low-temperature LD spectrum of *C. tepidum* has been available (Melkozernov et al. 1998) and it has become apparent that the overall shape of the low-temperature LD of the two complexes is very similar. Based on our discussion on the correlation between the orientations of the BChl dipole moments and the shape of the LD spectrum, it is highly probable that the trends in the positions of the BChl site energies are conserved to a large extent. It is interesting to note that the most different BChls are involved in the pairwise interactions (BChl 1-BChl 2 and BChl 5-BChl 6) which are most likely to deviate from the point dipole approximation. It can be speculated that the differences in the spectra of the two species may stem primarily from the modifications on the interactions and the site energies of these particular BChls. Mutants of FMO complexes may be used to probe this speculation.

Acknowledgements Based in part on a thesis (by E. I. I.) submitted to the Middle East Technical University in partial fulfillment of the degree of Master of Science (June 1998).

References

Amerongen H van, Struve WS (1991) Excited state absorption in bacteriochlorophyll *a* protein from the green photosynthetic bacterium *Prosthecochloris aestuarii:* reinterpretation of the absorption difference spectrum. J Phys Chem 95: 9020–9023

Amerongen H van, Grondelle R van (1995) Transient absorption spectroscopy in study of processes and dynamics in biology. Methods Enzymol 246: 201–225

Blankenship RE, Olson JM, Miller M (1995) Antenna complexes from green photosynthetic bacteria. In: Blankenship RE, Madigan MT, Bauer CE (eds) Anoxygenic photosynthetic bacteria. Kluwer, Dordrecht, pp 399–435

Buck DR, Savikhin S, Struve WS (1996) Ultrafast absorption difference spectra of the Fenna-Matthews-Olson protein at 19 K: experiment and simulations. Biophys J 72: 24–36

Buck DR, Savikhin S, Struve WS (1997) Effect of diagonal energy disorder on circular dichroism spectra of Fenna-Matthews-Olson trimers. J Phys Chem B 101: 8395–8397

Fenna RE, Matthews BW (1975) Chlorophyll arrangement in a bacteriochlorophyll protein from *Chlorobium limicola*. Nature 258: 573–577

Fleming GR, Grondelle R van (1994) The primary steps of photosynthesis. Phys Today 47: 48–55

Förster T (1965) Delocalization of excitation and excitation transfer. In: Sinanoglu O (ed) Part II. B.1 of Modern quantum chemistry: Istanbul lectures, part III. Action of light and organic crystals. Academic Press, New York, pp 93–137

Freiberg A, Lin S, Tipmann K, Blankenship RE (1997) Exciton dynamics in FMO bacteriochlorophyll proteins at low temperatures. J Phys Chem B 101: 7211–7220

Grondelle R van, Dekker JP, Gillbro T, Sundström V (1994) Energy transfer and trapping in photosynthesis. Biochim Biophys Acta 1187: 1–65

Gülen D (1996) Interpretation of the excited state structure of the Fenna-Matthews-Olson pigment complex of *Prosthecochloris aestuarii* based on the simultaneous simulation of the 4 K absorption, linear dichroism and singlet-triplet absorption difference spectra: a possible excitonic explanation? J Phys Chem B 100: 17683–17689

Iseri EI (1998) Electronic excited states and excitation transfer kinetics in the FMO protein complex of the photosynthetic bacterium *Prosthecochloris aestuarii* at low temperatures. MS Thesis, Middle East Technical University, Ankara, Turkey

Iseri EI, Gülen D (1997) Absorption and linear dichroism of the Fenna-Matthews-Olson pigment-protein complex of *Prosthecochloris aestuarii*: an exciton model. Doğa-Tr J Phys 21: 1129–1143

Jean JM, Chan CK, Fleming GR (1988) Electronic energy transfer in photosynthetic bacterial reaction centers. Isr J Chem 28: 169–175

Johnson SG, Small GJ (1991) Excited state structure and energy transfer dynamics of the bacteriochlorophyll *a* antenna complex from *Prosthecochloris aestuarii*. J Phys Chem 95: 471–479

Kenkre VM, Knox RS (1974) Theory of fast and slow excitation transfer rates. Phys Rev Lett 33: 803–806

Knox RS (1975) Excitation energy transfer and migration: theoretical considerations. In: Govindjee (ed) Bioenergetics of photosynthesis. Academic Press, New York, pp 183–221

Knox RS, Gülen D (1993) Theory of polarized fluorescence from molecular pairs: Förster transfer at large electronic coupling. Photochem Photobiol 57: 40–43

Krueger BP, Scholes GD, Fleming GR (1998) Calculation of couplings and energy-transfer pathways between the pigments of LH2 by ab initio transition density cube method. J Phys Chem B 102: 5378–5386

Leegwater AJ, Durrant RD, Klug DR (1997) Exciton equilibration induced by phonons: theory and its application to PS II reaction centers. J Phys Chem B 101: 7205–7210

Li Y, Zhou W, Blankenship RE, Allen JP (1997) Crystal structure of the bacteriochlorophyll *a* protein from *Chlorobium* tepidum. J Mol Biol 271: 456–471

Louwe RJW, Vrieze J, Hoff AJ, Aartsma TJ (1997 a) Towards an integral interpretation of the optical steady-state spectra of the FMO complex of *Prosthecochloris aestuarii*. II. Exciton simulations. J Phys Chem B 101: 11273–11279

Louwe RJW, Aartsma TJ, Hoff AJ (1997 b) Towards an integral interpretation of the optical steady-state spectra of the FMO complex of *Prosthecochloris aestuariii*. I. An investigation with linear-dichroic absorbance-detected magnetic resonance. J Phys Chem B 101: 11280–11287

Lu X, Pearlstein R (1993) Simulations of *Prosthecochloris* bacteriochlorophyll *a* protein optical spectra improved by parametric computer search. Photochem Photobiol 57: 86–91

Melkozernov AN, Olson J, Li Y-F, Allen JP, Blankenship RE (1998) Orientation and excitonic interactions of the Fenna-Matthews-Olson bacteriochlorophyll *a* protein in membranes of the green sulphur bacterium *Chlorobium tepidum*. Photosynth Res 56: 315–328

Mourik F van, Verwijst RR, Mulder JM, Grondelle R van (1994) Singlet-triplet spectroscopy of the light-harvesting BChl *a* complex of *Prosthecochloris aestuarii*. J Phys Chem 98: 10307–10312

Olson JM, Ke B, Thompson KH (1976) Exciton interaction among chlorophyll molecules in bacteriochlorophyll *a* protein and bacteriochlorophyll *a* reaction center complexes from green bacteria. Biochim Biophys Acta 430: 524–537

Pearlstein RM (1991) Theoretical interpretation of antenna spectra. In: Scheer H (ed) Chlorophylls. CRC Press, Boca Raton, pp 1047–1078

Pearlstein RM (1992) Theory of the optical spectra of the bacteriochlorophyll *a* antenna protein trimer from *Prosthecochloris aestuarii*. Photosynth Res 31: 213–226

Phillipson KD, Sauer K (1972) Exciton interaction in a bacterio chlorophyll protein from *Chloropseudomonas ethylica*. Absorption and circular dichroism at 77 K. Biochemistry 11: 1880–1885

Savikhin S, Struve WS (1994) Ultrafast energy transfer in FMO trimers from the green bacterium *Chlorobium tepidum*. Biochemistry 33: 11200–11208

Savikhin S, Struve WS (1996) Low-temperature energy transfer in FMO trimers from the green photosynthetic bacterium *Chlorobium tepidum*. Photosynth Res 48: 271–276

Savikhin S, Buck DR, Struve WS (1997) Pump-probe anisotropies of Fenna-Matthews-Olson protein trimers from *Chlorobium tepidum*: a diagnostic for exciton localization? Biophys J 73: 2090–2096

Struve WS (1995) Theory of electronic energy transfer. In: Blankenship RE, Madigan MT, Bauer CE (eds) Anoxygenic photosynthetic bacteria. Kluwer, Dordrecht, pp 297–313

Tronrud DE, Schmidt MF, Matthews BW (1986) Structure and X-ray amino acid sequence of a bacteriochlorophyll *a* protein from *Prosthecochloris aestuarii* refined at 1.9 Å resolution. J Mol Biol 188: 443–454

Vasmel H, Amesz J, Kramer HJM, Swarthoff T (1983) Isolation and properties of a pigment-protein complex associated with the reaction center of the green photosynthetic sulfur bacterium *Prosthecochloris aestuarii*. Biochim Biophys Acta 725: 361–367

Vulto SIE, Streltsov AM, Aartsma TJ (1997) Excited state energy relaxation in the FMO complexes of the green bacterium *Prosthecochloris aestuarii* at low temperatures. J Phys Chem B 101: 4845–4850